Korean J. Chem. Eng., 40(6), 1340-1352 (2023)
DOI: 10.1007/s11814-023-1381-7

pISSN: 0256-1115
eISSN: 1975-7220

Thermodynamic, economic, as well as risk and reliability analyses of a molten carbonate fuel cell-based combined cooling, heating, and power system

Mahmood Mehregan*,†, Seyyed Mahdi Miri*, Seyed Majid Hashemian*, Mohammad Mahdi Balakheli*, and Aras Amini**

*Faculty of Mechanical Engineering, Shahrood University of Technology, Shahrood, Iran, P.O.B. 3619995161
**The Faculty of Sciences of Orsay, Université Paris-Saclay, Orsay, France
(*Received 18 August 2022 • Revised 12 December 2022 • Accepted 18 December 2022*)

Abstract−A complete thermodynamic analysis of a novel combined cooling, heating, and power (CCHP) system based on molten carbonate fuel cell (MCFC) as the prime mover, single-effect water-lithium bromide absorption chiller, polymer fuel cell (PEMFC), as well as heat and hydrogen storage tanks, has been performed. Risk and reliability analyses were performed, which are two of the most significant achievements that have not been previously examined in similar studies. A thermodynamic analysis was performed on three scenarios, and one of them revealed an energy efficiency of 87.85% and exergy efficiency of 86.62% for the hybrid CCHP system. Also, the results indicated that increasing the fuel consumption factor decreases the M-factor (ratio of production power to the total power and heat production in the fuel cell) and output hydrogen from the MCFC. The results of system reliability and risk analyses indicate that the mean times to the first failure of the MCFC, PEMFC, and absorption chiller are 19459.57, 1404.04, and 86104.07 working hours under normal conditions, respectively. In one of the scenarios, the calculated amount of economic efficiency and payback period of investment by calculating the inflation rate are 6.3% and 3.1 years, respectively.

Keywords: Risk and Reliability Analysis, Energy and Exergy Analysis, Molten Carbonate Fuel Cell, Polymer Fuel Cell, Economic Analysis, CCHP

INTRODUCTION

Over the past few decades, combined generation systems have increasingly gained engineers' and consumers' attention due to improving energy efficiency and reduced costs. The use of combined systems providing power, heat, and cold is one way to utilize the maximum energy and exergy of the system. In such systems, as a prime mover produces power, some heat is released. The efficiency of a system will not increase unless the heat released from the system retains the system. To retain the heat, the use of an absorption chiller is recommended. If a portion of the heat is used for heating and the rest is used for cooling demand, as in combined heating, cooling, and power (CCHP) systems, the efficiency of the system is significantly higher than that of a conventional CHP system.

Depending on the type of absorption chiller, including single, double, and three-effect chillers, the efficiency of absorption chillers varies from 0.6 to 1.9. These systems are applicable in various industrial settings, including factories, large companies that manufacture of industrial components for residential and commercial buildings, hospitals, and power plants. Additionally, these systems incorporate a variety of prime movers, including internal and external combustion engines, fuel cells, and turbines; each of them is designed and selected based on the amount of energy required on-site and the practical requirements of the desired mover.

†To whom correspondence should be addressed.
E-mail: mehregan@shahroodut.ac.ir

The working procedure of these systems is the use of waste heat for cooling and heating demand, leading to an increase in system efficacy. Numerous studies have been conducted in this area regarding simultaneous generation so far, but none of them consider all aspects of thermodynamics as well as risk and reliability analyses.

Sheykhi et al. [1] evaluated the thermodynamic, economic, and environmental performance of a hybrid CCHP system powered by a Stirling engine. Their study showed that output power, waste heat, and exergy destruction reach their highest level at high engine frequencies. In another study, Sheykhi et al. [2] analyzed a cogeneration system based on internal and external combustion engines. Return on investment (ROI) of the system was calculated under various operating conditions. Liu et al. [3] investigated an operating strategy for the part-load performance of a combined cycle cogeneration power plant. Their research recovered some of the heat from combustion gases in a heat recovery steam generator (HRSG) and manipulated the turbine's inlet guide vanes, thereby regulating the turbine's part-load operation. The results indicated that carbon dioxide emissions were reduced up to 13.8 kg/MWh. Accordingly, Wu et al. [4] analyzed a hybrid cycle of molten carbonate fuel cells with a thermoelectric system to generate power and cooling.

Ahn et al. [5] proposed a novel technique to estimate the efficiency of a hybrid system of a micro-gas turbine and a molten carbonate fuel cell (MCFC), including carbon capture and off-gas recirculation. The efficiency of their system was determined to be 57%. A CCHP system was introduced by Marefati et al. [6]. Their system was powered by a molten carbonate fuel cell. A solar collector was integrated into the system via the carbon dioxide capture

process. Their system produced 81 MW of power.

Energy, exergy, and economic efficiencies of a molten carbonate fuel cell-based power generation system were analyzed and modeled along with an organic Rankine cycle (ORC). Roy et al. [7] determined that their fuel cell could generate 105.3 kW of power, and energy efficiency was determined to be 38.49%

Ghorbani et al. [8] introduced a CCHP system with a molten carbonate fuel cell as the prime mover and a multi-effect desalination system with a single-effect ammonia-water absorption chiller. The exergy efficiency of the whole system was calculated to be 88.95%. Wang et al. [9] analyzed the energy, exergy, and environmental impacts of a CCHP system integrated with a concentrated photovoltaic system and heat generation via thermal collectors. The energy efficiency values of the hybrid system in two modes of cooling and heating were obtained as 63.3% and 61.8%, respectively. Rajabi et al. [10] conducted a review on a chemical loop of CCHP. According to the results, systems containing molten carbonate fuel cells were 60-70% efficient.

Mastropasqua et al. [11] researched retrofitting MCFCs to capture carbon dioxide and rise of production of energy in the steel industry. The system decreased carbon dioxide emissions by 70%, enough to generate 545 MW of energy.

Erzen et al. [12] evaluated the biogas-fueled MCFC-thermophotovoltaic CCHP system. The maximum output power of the system was 16.14 kW. Salehi et al. [13] presented energy, exergy, and environmental analyses of a cogeneration system using an MCFC, a Stirling engine, and an ORC. The Stirling engine and the ORC were started using the waste heat from the fuel cell. The highest rate of exergy destruction was related to the MCFC. Spinelli et al. [14] evaluated the ability of MCFCs to capture carbon in two different scenarios for combined-cycle natural gas power plants. They examined the voltage drop that occurs during the carbon capture process.

In another study, Açıkkalp et al. [15] compared the performance of a metal thermal electric converter (MTEC) and a thermoelectric generator (TEG) to use the output heat from an MCFC. The estimated output power was calculated for MCFC-MTEC and MCFC-TEG as well as the system efficiency under different conditions. Wejrzanowski et al. [16] designed porous electrodes for MCFCs using a microstructure-driven approach. According to the results, using commercial nickel as the cathode's gas side layer increased output power and decreased the fragility of electrode elements.

Moreover, Ryu et al. [17] analyzed the thermal evaluation of a hybrid MCFC system with a supercritical carbon dioxide (s-CO2) power cycle and district heating system. The analysis revealed that when the hybrid system is used, the energy efficiency increases by up to 4.6% compared to when the cell is used alone. Ahn et al. [18] concluded that an MCFC with a gas turbine performs better than a steam turbine after evaluating a hybrid MCFC system with a gas turbine and a steam turbine.

Guo et al. [19] performed performance optimization of a combined system including an MCFC and a Two-stage thermoelectric generator (TTEG). They demonstrated that the highest power density of MCFCs with a TTEG is 16.9% higher than that for a single MCFC. Ricardo et al. [20] developed a combined heat and power system based on an MCFC as a prime mover using biogas. The main purpose of their study was to reduce environmental pollution. The fuel cell was supplied with fuel via a standard sewage gas system. They assessed the economic analysis of the system using the Monte Carlo method.

The design and optimization of CCHP systems concerning operational flexibility were evaluated by Wang et al. [21]. Also, energy, economic, and environmental performance of the CCHP system was evaluated. Rosen et al. [22] evaluated the performance of an MCFC for CO2 capture from flue gas from a natural gas combined cycle. Peng et al. [23] performed energy and exergy analyses of a combined system of solar collector and solid oxide fuel cell (SOFC) in a CCHP system. The highest efficiency obtained in this system was calculated as 37.33%. Thermodynamic analysis for evaluating the energy and exergy performances of a CCHP system with a polymer electrolyte membrane (PEM) fuel cell with a single-effect absorption chiller was evaluated by Chahartaghi and Kharkeshi [24]. They estimated the exergy and energy efficiencies of the system as about 55% and 82%, respectively. Chahartaghi et al. [25] evaluated the performance of a trigeneration system that utilized phosphoric acid fuel cells in conjunction with an organic Rankine cycle. The trigeneration system outperforms the phosphoric acid fuel cell alone by 57% in terms of energy efficiency and 5.3% in terms of exergy efficiency.

The current study developed a CCHP system aligned with an MCFC, a PEM fuel cell, and a single-effect absorption chiller. In comparison to previous research, the PEM fuel cell was used for the first time in that its fuel is obtained from debris from the MCFC fuel cell's outlet gases. As a result, the behavior of the entire introduced system is observed by adding a new component, the PEM fuel cell.

Given that the excess hydrogen produced by an MCFC has not been utilized in the previous studies, in the present research, the hydrogen produced by a molten carbonate fuel cell has been investigated for the first time in three scenarios. On the other hand, this study introduces the M-factor as a novel concept, incorporating the ratio of production power to total power and heat production in the fuel cell to evaluate changes in the fuel consumption factor for the first time. Additionally, because reliability and risk analyses of system components have not been performed previously, this work performed the first analysis of the system components to predict the number of failures and system performance reliability. Also, a comprehensive economic analysis was conducted in this paper, which includes the factors of return on investment in normal conditions and with the inflation rate, net present value (NPV), annual profit, end-of-life scrap value, future and present values of money and investment efficiency.

SYSTEM AND SCENARIO DESCRIPTION

This study evaluated a new CCHP system with a molten carbonate fuel cell as a prime mover. Fig. 1 illustrates the cycle presented in this research. In scenario one, the power generated by the MCFC reaches consumers, in which case the MCFC releases some hydrogen. In scenario two, the hydrogen which was made by the MCFC is used to run a polymer fuel cell. The system incorporates a single-effect absorption chiller to utilize waste heat generated by the MCFC. Some waste heat enters the absorption chiller to generate cooling, and the remaining heat enters the building to supply hot

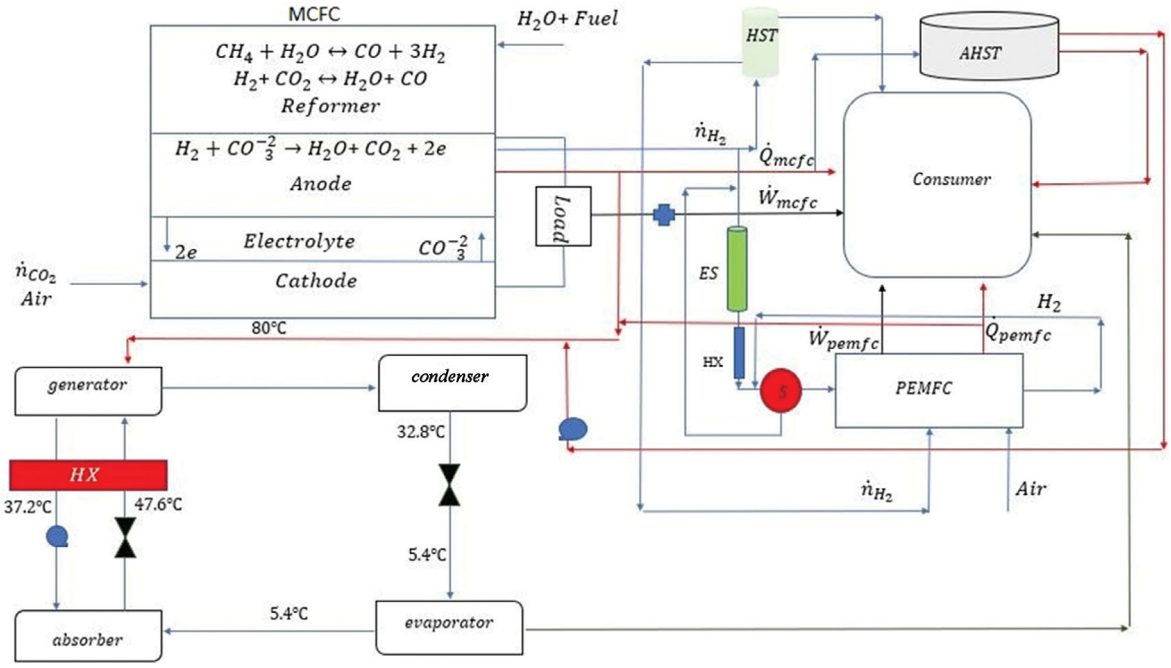

Fig. 1. Block diagram of the hybrid CCHP process.

water or heating. In case of need, heat generated by the polymer fuel cell can be used in the circuit. Likewise, some of the excess hydrogen produced by the MCFC is stored in a tank. The required hydrogen for the polymer fuel cell is purchased in scenario three, and any excess hydrogen generated by the molten carbonate is not recovered or used. All three scenarios have thoroughly evaluated miscellaneous points of view of energy, exergy, and economic assessments. Note that all detailed specifications about the MCFC, PEMFC, and absorption chiller are considered.

ENERGY MODEL

1. MCFC

A fuel cell is an electrochemical system that converts chemical energy directly into electrical energy. The carbonate ion produced by an electrochemical reaction is transferred from cathode to anode via an electrolyte. At the anode pole, the hydrogen produced through the reforming and shift reactions by the reformer will combine with the carbonate ions transferred from the cathode, producing water, carbon dioxide, and electrons as output. The electrons are transferred from the anode to the cathode by passing through the catalysts via an external circuit and generating electricity. By combining the half-reactions of the anode and cathode, an overall electrochemical reaction is obtained inside the fuel cell, which is exothermic, and its heat can be used to supply the energy required for the reforming reaction. The reforming, shift, anode, and total electrochemical reactions are performed according to Eqs. (1) to (4), respectively:

$$CH_4 + H_2O \rightarrow CO + 3H_2 \quad (1)$$

$$CO + H_2O \rightarrow CO_2 + H_2 \quad (2)$$

$$H_2 + CO_3^{2-} \rightarrow H_2O + CO_{2,a} + 2e^- \quad (3)$$

$$H_2 + \frac{1}{2}O_2 + CO_{2,c} \rightarrow H_2O + CO_{2,a} \quad (4)$$

The power generated is calculated using Eq. (5).

$$W = 0.965 \times N \times I \times V \quad (5)$$

where N denotes the number of cells in the desired stack, and V denotes the voltage of the MCFC. The voltage and current are calculated from Eqs. (6) and (7), respectively [6,26]. The inverter efficiency is considered to be 0.965%.

$$V_{cell} = E_{nerst} - (R_{an} + R_{ca} + R_{ohmic}) \times i \quad (6)$$

$$I = i \times A \quad (7)$$

where i represents current density in ampere per square meter, and A denotes the active surface of the fuel cell in a square meter. In the V_{cell} equation, the actual voltage, E_{nerst} is the ideal return voltage, calculated using Eq. (8) [27]:

$$E_{nerst} = \left(\frac{\Delta G}{n_e \times F}\right) + \left(\frac{RT}{n_e \times F}\right) \times \ln\left(\frac{P_{H_2,an} \times P_{O_2,ca}^{0.5} \times P_{CO_2,ca}}{P_{H_2O,an}^{1} \times P_{CO_2,an}^{1}}\right) \quad (8)$$

n denotes the number of electrons released from the hydrogen molecule (equal to 2), and F is the Faraday constant (96,487 C/mol). The cell resistance losses, including ohmic, cathode, and anode resistances, are calculated according to Eqs. (9) to (11), respectively [28]:

$$R_{ohmic} = 0.5 \times 10E\text{-}4 \times \exp\left(3{,}016 \times \left(\frac{1}{T} - \frac{1}{923}\right)\right) \quad (9)$$

$$R_{ca} = 7.505 \times 10E\text{-}10 \times \exp\left(\frac{E_{ac_{ca}}}{RT}\right) \times (p_{O_2,ca}^{-0.43}) \times (p_{CO_2,ca}^{-0.09}) \quad (10)$$

$$R_{an} = 2.27 \times 10E\text{-}9 \times \exp\left(\frac{E_{ac_{an}}}{RT}\right) \times (p_{H_2,an}^{-0.42}) \times (p_{CO_2,an}^{-0.17}) \times (p_{H_2O,an}^{-1}) \quad (11)$$

Gibbs free energy changes in a molten carbonate fuel cell depend on the reaction temperature as determined by Eq. (12). In these equations, $p_{i,an,ca}$ and n_e denote partial pressure and the number of released electrons, respectively [29].

$$\Delta G = 242{,}000 - 45.8T \tag{12}$$

2. PEMFC

In a PEM fuel cell, the electrolyte consists of a thin polymer membrane mainly made of Nafion with proton permeation. The core of the fuel cell is a proton-conducting polymer. A platinum catalyst supported on porous carbon is commonly used in electrodes to connect both sides of the electrolyte to each other.

Eqs. (13) to (15) present the reactions of PEM fuel cells [30]:

$$\text{Anode: } H_2 \rightarrow 2H^+ + 2e^- \tag{13}$$

$$\text{Cathode: } 2H^+ + 2e^- + 0.5O_2 \rightarrow H_2O + \text{Heat} \tag{14}$$

$$\text{Overall reaction: } H_2 + 0.5O_2 \rightarrow H_2O + \text{Heat} + W \tag{15}$$

The hydrogen consumption rate in the cell can be obtained through the molar flow rate balances via Eq. (16):

$$\dot{n}_{H_2,\,cons} = N_{cell}\frac{iA}{2F} \tag{16}$$

The actual voltage must be calculated to determine the rate of the fuel cell. The open-circuit voltage, otherwise known as the Nernst voltage, is obtained by Eq. (17) [30]:

$$E_{Nernst} = \frac{-\Delta G^0}{n_e F} + \frac{R_u T_{fc}}{n_e F}\ln\left(\frac{P_{H_2}\sqrt{P_{O_2}}}{P_{H_2O}^{sat}}\right) \tag{17}$$

In Eq. (17), E_{Nernst} denotes the Nernst voltage, ΔG is the Gibbs free energy change, n_e is the number of electrons transferred to the fuel cell, F is the Faraday constant, R_u is the universal gas constant, and T_{fc} is the operating temperature of the fuel cell. P_{H_2} and P_{O_2} are the effective partial pressures of hydrogen and oxygen, respectively; and $P_{H_2O}^{sat}$ is the saturation pressure of water. Due to irreversible losses in the fuel cell, the actual voltage is lower than the Nernst voltage. These losses are caused by excessive ohmic voltage losses, concentration, as well as activation. The actual output voltage of the fuel cell can be determined by Eq. (18) [14]:

$$V_{fc} = E_{nernst} - V_{conc} - V_{ohm} - V_{act} \tag{18}$$

Should the current density of the fuel cell increase, the partial pressures of oxygen and hydrogen will be reduced. Under such conditions, current density performance does not correspond to the reactant concentration. This overvoltage occurs at high current densities, and these irreversible losses are calculated through Eq. (19) [14]:

$$V_{conc} = \frac{RT_{fc}}{n_e F}\ln\left(\frac{i_L}{i_L - 1}\right) \tag{19}$$

Excessive ohmic voltage results from electrical resistance in the fuel cell. This excessive voltage is defined by Eq. (20): [9].

$$V_{ohm} = IR_{int} \tag{20}$$

Under Ohm's law, R_{int} represents the total internal resistance, which is a function of current and temperature; hence, there is a relation for this resistance written by Eq. (21) [9]:

$$R_{int} = \frac{r_{mem}L}{A_{cell}} \tag{21}$$

r_{mem} denotes membrane resistance. Proportionally, there is an experimental relationship for the resistance of a Nafion membrane, denoted by Eq. (22) [9]:

$$r_{mem} = \frac{181.6\left(1 + 0.03i + 0.062\left(\frac{T_{fc}}{303}\right)^2 (i^{2.5})\right)}{11.866 - (3i)\exp\left(4.18\left(1 - \frac{303}{T_{fc}}\right)\right)} \tag{22}$$

There are two types of active overvoltage in PEMFCs: anode as well as cathode. In this manner, the anode one would be ignored; however, the active one is critical for charging movement through the electrode. This parameter is calculated using Eq. (23) [14,27]:

$$V_{act} = -[-0.948 + \varepsilon T_{fc} + 0.000076T_{fc}(\ln(I)) - 0.000193T_{fc}(\ln(C_{O_2,\,conc}))] \tag{23}$$

$$\varepsilon = 0.00286 = 0.0002\ln(A_{cell}) + 0.000043\ln(C_{H_2,\,conc}) \tag{24}$$

In Eqs. (23) and (24), I represents the fuel cell current, $C_{O_2,\,conc}$ and $C_{H_2,\,conc}$ are oxygen and hydrogen concentrations, respectively, which are calculated using Henry's Law through Eqs. (25), (26) as follows [14]:

$$C_{O_2,\,conc} = 1.97 * 10^{-7} P_{O_2}\exp\left(\frac{498}{T_{fc}}\right) \tag{25}$$

$$C_{H_2,\,conc} = 9.174 * 10^{-7} P_{H_2}\exp\left(\frac{-77}{T_{fc}}\right) \tag{26}$$

After the output voltage is calculated, the produced power of the fuel cell is expressed by Eq. (27):

$$W_{fc} = N_{cell}V_{fc}I \tag{27}$$

3. Absorption Chiller

Eqs. (28) to (31) are established to analyze the absorption chiller's heat exchanger [1].

$$Eff_{hx} = \frac{T_4 - T_5}{T_4 - T_2} \tag{28}$$

$$C_{hot} = m_4 \cdot \left[\frac{h_4 - h_5}{T_4 - T_5}\right] \tag{29}$$

$$C_{cold} = m_2 \cdot \left[\frac{h_3 - h_2}{T_3 - T_2}\right] \tag{30}$$

$$Q_{hx} = m_1 \cdot (h_3 - h_2) = m_4 \cdot (h_4 - h_5) \tag{31}$$

In Eqs. (28) to (31), Eff_{hx} denotes the efficiency of the heat exchanger and Q_{hx} is heat rate exchanging in the heat exchanger. Eqs. (32) to (34) are related to the generator.

$$m_3 = m_4 + m_7 \tag{32}$$

$$m_3 x_3 = m_4 x_4 \tag{33}$$

$$m_3 h_3 - m_4 h_4 - m_7 h_7 + Q_d = 0 \tag{34}$$

In Eqs. (32) to (34), x is the concentration, and Q_d is the heat rate transferring from the working fluid to the generator. Eqs. (35)

to (38), respectively, are related to the condenser, valve, and evaporator of the absorption chiller.

$$Q_{con} = m_7(h_7 - h_8) \tag{35}$$

$$Q_{eva} = m_9(h_{10} - h_9) \tag{36}$$

$$m_{10}h_{10} + m_6h_6 - Q_{abs} - m_1h_1 = 0 \tag{37}$$

$$COP = \frac{Q_{eva}}{Q_d} \tag{38}$$

4. Energy Efficiency

Eqs. (39) to (41) are related to the cycle and applied to calculate the energy efficiency of the system [24,30]:

$$\eta_{elec} = \frac{\Sigma \dot{W}_i}{\dot{m}_{fuel,\,in} \cdot LHV} \tag{39}$$

$$\eta_{CHP} = \frac{\Sigma \dot{W}_i + \Sigma \dot{Q}_{i,\,H}}{\dot{m}_{fuel,\,in} \cdot LHV} \tag{40}$$

$$\eta_{CCHP} = \frac{\Sigma \dot{W}_i + \Sigma \dot{Q}_{i,\,H} + \Sigma \dot{Q}_{i,\,C}}{\dot{m}_{fuel,\,in} \cdot LHV} \tag{41}$$

In Eqs. (39) to (41), subscripts of *i*, H, and C represent specific components, heating, and cooling, respectively.

EXERGY MODEL AND M-FACTOR

1. Control Volume

The control volume is the part of the system which should be evaluated. For a control volume, exergy analysis is performed using Eq. (42) [32]:

$$\Sigma \dot{E}X_{in} - \Sigma \dot{E}X_{out} + \Sigma_k \dot{E}X^Q - \Sigma_k \dot{E}X^w - \Sigma \dot{E}X_{dest} = 0 \tag{42}$$

In Eq. (42), $\Sigma \dot{E}X_{in}$, $\Sigma \dot{E}X_{out}$, $\Sigma_k \dot{E}X^Q$ and $\Sigma_k \dot{E}X^w$ represent the input rate of exergy, the output rate of exergy, exergy transferred by heat, and exergy transferred by work, respectively. Also, $\Sigma \dot{E}X_{dest}$ denotes irreversibility or exergy destruction. The term $\dot{E}X$ is defined by Eq. (43):

$$\dot{E}X = \dot{m}(ex_{ph} + ex_{ch} + ex_{kn} + ex_{pt}) \tag{43}$$

The physical exergy is calculated by Eq. (44). h and s represent enthalpy and entropy, respectively. Furthermore, zero subtitle means a dead state or environmental conditions. In the case of an ideal gas, Eq. (44) appears in the form of Eq. (45) [33]:

$$ex_{ph} = (h - h_0) - T_0(s - s) \tag{44}$$

$$ex_{ph} = c_p T_0 \left[\frac{T}{T_0} - 1 - \ln\left(\frac{T}{T_0}\right) + \ln\left(\frac{p}{p_0}\right)^{\frac{k-1}{k}} \right] \tag{45}$$

$$ex_{ch} = \Sigma x_n \times ex_{ch}^n + RT_0 \Sigma x_n \ln x_n \tag{46}$$

The chemical exergy [34] is calculated using Eq. (46). In this equation, x_n denotes the mass fraction of components, and ex_{ch}^n denotes the standard chemical exergy of the component of n.

The exergy transferred by work and heat is calculated using Eqs. (47) and (48):

$$\dot{E}X_i^{\dot{W}} = \dot{W}_i \tag{47}$$

$$\dot{E}X_i^{\dot{Q}} = \dot{Q}_i \times \left(1 - \frac{T_0}{T_i}\right) \tag{48}$$

2. Exergy Efficiency

Should a fuel cell generate only electricity, Eq. (49) will calculate the exergy efficiency of the fuel cell:

$$\eta_{ex,\,elec} = \frac{\Sigma \dot{E}X_i^{\dot{W}}}{(ex_{ph} + ex_{ch})_{fuel,\,in} \cdot \dot{m}_{fuel,\,in}} \tag{49}$$

In this equation, $\eta_{ex,\,elec}$ denotes the electrical exergy efficiency of a fuel cell. Furthermore, the exergy efficiencies for CHP and CCHP types are calculated by Eqs. (50) and (51) [24]:

$$\eta_{ex,\,CHP} = \frac{\Sigma \dot{E}X_i^{\dot{W}} + \Sigma \dot{E}X_i^{\dot{Q}_H}}{(ex_{ph} + ex_{ch})_{fuel,\,in} \cdot \dot{m}_{fuel,\,in}} \tag{50}$$

$$\eta_{ex,\,CCHP} = \frac{\Sigma \dot{E}X_i^{\dot{W}} + \Sigma \dot{E}X_i^{\dot{Q}_H} + \Sigma \dot{E}X_i^{\dot{Q}_C}}{(ex_{ph} + ex_{ch})_{fuel,\,in} \cdot \dot{m}_{fuel,\,in}} \tag{51}$$

3. M-Factor

The M-Factor, a comprehensive analysis to assess the changes in power and heat, is calculated using Eq. (52) and is defined as the ratio of production power to the total production of power and heat in a CHP system. To point out more, if the produced heat or power is not available, the unknown quantity will be reached via the M factor. In this study, the M- factor was introduced as a new factor for the first time. The larger M-factor value results in the higher generated power in proportion to the power and heat generated by the CHP in scenario one.

$$M_{factor} = \frac{\Sigma \dot{W}_{MCFC}}{\Sigma(\dot{W}_{MCFC} + \dot{Q}_{MCFC})} \tag{52}$$

ECONOMIC ANALYSIS

1. Simple Interest

Borrowers pay interest to lenders for loans, which is the cost of borrowing money. Th e simple interest is a fixed percentage of the principal borrowed or lent over a certain period. The simple interest is calculated on the initial of money. The rates are expressed as fixed percentages of borrowed loans. In this way, the total repayment value (TRV) is presented by Eq. (53) [35]:

$$TRV = LV \times \left(\frac{IR}{100} \times LV \times p\right) \tag{53}$$

where TRV denotes the total repayment value, LV is the initial loan value, IR is the interest rate, and p represents the repayment period (years).

2. Compound Interest

Due to compound interest, borrowers must pay interest on interest as well as principal, as it accrues and is added to previous periods' interest. Compound interest is evaluated by the initial loan and the accumulated interest of previous periods. It is calculated by Eq. (54):

$$TRV = LV \times \left(1 + \frac{IR}{100}\right)^p \tag{54}$$

3. Real and Discounted Payback Period

The discounted payback period is used to determine a project's

profitability. By discounting future cash flows and recognizing the time value of money, it is possible to determine how long it will take to break even.

The payback period is defined as a ratio of capital cost to the annual net saving. This parameter is shown in Eq. (55).

$$PB = \frac{CC}{AS} \tag{55}$$

$$DPP = Ln\left(\frac{1}{1-\frac{CC\times r}{AS}}\right) \div Ln(1+r) \tag{56}$$

In Eqs. (55) and (56), discounted payback period (DPP) is the rate of return on investment by considering the rate of inflation. Likewise, the payback period (PB) is the return on investment, CC is the initial capital cost, and AS is the annual net savings.

4. The Present Value of Investment Capital and its Net Present Value at the end of the Project's Life

With a specified rate of return, present value (PV) represents the current value of a future sum of money or stream of cash flows. The present value and net present value of capital cost at the end of the project's life are presented in Eqs. (57) and (58), respectively.

$$PV = S\times\left(1+\frac{IR}{100}\right)^{-n} \tag{57}$$

$$NPV = \sum_{i=0}^{n} PV \tag{58}$$

The net present value method considers that a cash saving (often referred to as a 'cash flow') of 1000 Euros in year 10 of a project will be worth less than a cash flow of 1000 Euros in year 2.

PV, S, an NPV represent the present value, the amount of investment, and the sum of investment values in n years, respectively.

5. Future Value of Money

Future value describes what money will be worth in the future. Typically, cash in a savings account or a hold in a bond purchase earns compound interest and so has a different value in the future. The future value would grow as compound interest is added after n years, it can be calculated by Eq. (59):

$$FV = D\times\left(1+\frac{IR}{100}\right)^{n} \tag{59}$$

In Eq. (59), FV represents the future value of money after n years. The components used in a cogeneration system are sold after the end of their life as scrap products. Accordingly, the system is sold at the end of its lifespan under a coefficient of the initial investment.

6. Cost Efficiency

Given that efficiency is defined as a ratio of total output to total input, cost efficiency can be defined mathematically using Eq. (60).

$$\eta_{eco} = \frac{\Sigma_{i=0}^{n} AS}{CC} \tag{60}$$

Table 1 contains the input assumptions of economic analysis [35-38].

Table 1. Input assumptions of economic analysis

Component	Price	Unit
Installation MCFC	3,300	$/kW
Installation PEMFC	2,700	$/kW
Chiller Costs	160	$/kW
Methane fuel Costs	0.163	$/Kg
Cells Maintenance and Repair	0.0125	$/Kwh
Chiller Maintenance and Repair	0.001	$/Kwh

RISK AND RELIABILITY ANALYSIS

Due to the lack of real data on the failure rate of working hours, risk and reliability analyses of each component were conducted in poor, average, and good operation working hours. By analyzing the reliability and risk of the system, it is important to mention that repairs are not considered a cost but rather managing physical resources. The reliability of a component is calculated mathematically by starting with the value of one. This value decreases until the failure time reaches the value of zero, named the end-of-life time of the components. When a device is completely recently developed and unused, the probability of its functioning as a faultless component is always the value one. Each of the components is expected to fail at least once during the device's lifetime if they operate during an average-operation working hours period. Additionally, the optimal rate of PB has been calculated by factoring in inflation. The operating hours of each component of the combined generation system were determined using EasyFit software, and thereby indicating the components follow a Weibull distribution function. To this end, this function is calculated using Eq. (61) [40]:

$$f(t) = \frac{\beta}{\eta}\times(t/\eta)^{\beta-1}\times\exp[-((t/\eta)^{\beta-1})] \tag{61}$$

In Eq. (61), β denotes the shape parameter, η is the scale parameter, and t is the corresponding variable, defined as each component's lifetime. Reliability is defined using Eq. (62):

$$R(t) = 1 - F(t) \tag{62}$$

where F(t) denotes the cumulative distribution of the Weibull function and is calculated using Eq. (63):

$$F(t) = \int_0^t f(t)dt \tag{63}$$

The number of system failures until the time of t is defined using Eq. (64):

$$E(N(t)) = \int_0^t h(t)dt \tag{64}$$

where h(t) is Hazard function and can be calculated by Eq. (65):

$$h(t) = \frac{f(t)}{R(t)} \tag{65}$$

Mean Time To Failure (MTTF) is expressed by Eq. (66):

$$MTTF = \int_0^\infty tf(t)dt = \int_0^\infty R(t)dt \tag{66}$$

Table 2. MCFC validation output results

Term	Value of present study	Ref. [27]	Difference
Output voltage (V)	0.689	0.699	1.43%
MCFC fuel cell efficiency (-)	46.6	47.3	1.47%
Output power (MW)	87.3272	88.5946	1.43%

Table 3. Polymer fuel cell validation output results

Term	Value of this paper	Ref. [24]	Difference
Output voltage (V)	0.6712	0.6613	1.4%
PEM fuel cell efficiency (-)	37.8	37.2	1.61%
Output power (kW)	39.2	38.66	1.3%

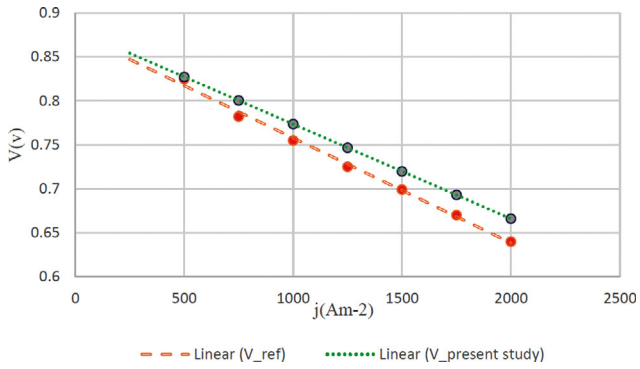

Fig. 2. Molten carbonate fuel cell validation diagram.

RESULTS AND DISCUSSION

Fig. 2 shows range of changes of voltage (V) versus the variations of the current density. According to Fig. 2 the change of the voltage with the current density has a similar behavior with reference [27] as well as good accuracy.

Also, Table 2 shows the output results based on a specific value of the operation condition for the present study and reference [27]. As it is clear, the results have good accuracy.

1. PEMFC Validation

The PEM fuel cell's performance was validated by comparing it to that of Ref. [24]. As demonstrated in Table 3, the current study is consistent with Ref. [24].

2. Absorption Chiller Validation

In this research, the validation of the absorption chiller was assessed using three key parameters, including coefficient of performance, output temperature of the evaporator, and output temperature of the condenser. As shown in Table 4, the validation of the absorption chiller which is used in this study is agreeable compared to that of the reference.

3. Flow Chart Description

In the present study, combined cooling, heating, and power system were modeled using EES and MATLAB software. The flowchart of the modeling can be seen in Fig. 3. In scenario one, a CCHP system with a molten carbonate fuel cell and an auxiliary heating source was presented. Accordingly, a single-effect water/lithium bromide absorption chiller was used to recover the output heat from the molten carbonate fuel cell. After reaching an appropriate temperature and working pressure, output hydrogen from the molten carbonate fuel cell enters the polymer fuel cell in scenario two. The excess hydrogen resulting from the molten carbonate fuel cell was also collected in a hydrogen storage tank. In the third scenario, the required hydrogen for the polymer fuel cell was

Table 4. Single effect absorption chiller validation output results

Term	Value of this research	Ref. [24]	Difference
COP	0.631	0.64	1.4%
T_{eva} (°C)	5.4	5.4	-
T_{Cond} (°C)	32.8	32.9	0.1 °C

Table 5. Input parameters used for CCHP system modeling

Symbol	Value [24,27,30]
MCFC fuel utilization factor, U_f	75%
MCFC CO2 utilization factor, U_{co2}	65%
MCFC Cell current density, i_c	1,500 (A/m^2)
Number of MCFC cells in the stack, N	2,000
MCFC total active area, A	0.3165 (m^2)
DC - AC efficiency	94%
Fuel molar flow rate, $\dot{n}_{fuel}$	40 (mol/s)
Cell operating pressure, P	1.13 (bar)
Natural gas LHV	37.3 (MJ/m^3)
MCFC operating temperature, T	923.3 (K)
Temperature of ambient, T	20 (°C)
Pressure of ambient, P	100 (kPa)
Cell numbers in the stack of PEMFC, N	4,720
PEMFC active surface area, A	0.0232 (m^2)
Operating pressure of PEMFC, P	113 (kPa)
Operating temperature PEMFC, T	80 (°C)
Current density of PEMFC, I	0.6 (A/cm^2)
The higher heating value of hydrogen, HHV	11.86 (MJ/m^3)
Hydrogen Stoichiometric rate	1.2
Air Stoichiometric rate	2
COP	0.631
Generator temperature	80 (°C)
Generator input heat rate	40 kW

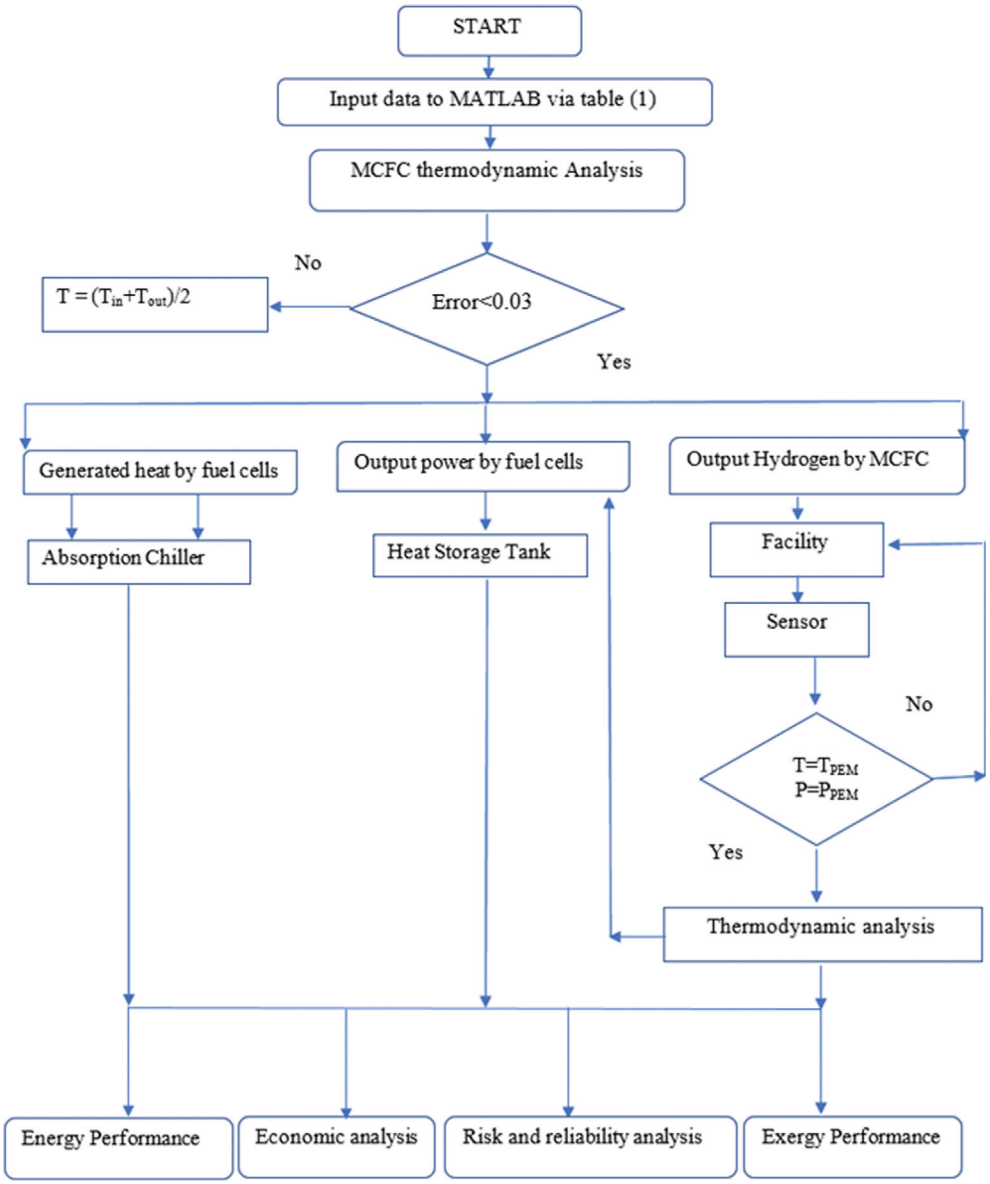

Fig. 3. The procedure for system modeling.

obtained from the market, and the output hydrogen from the molten carbonate was unrecovered. Numerous assessments were conducted in this paper, including analyses of energy, exergy, economics, reliability, and risk. For the first time, several critical parameters such as the current change of the MCFC, the system's energy and exergy efficiencies, the coefficient of performance of the absorption chiller, the payback period, the scrap costs of devices, the present and total values of investment at the end of life of the project, cost efficiency, mean time to the first failure, component reliability, and the number of expected failures of each component were also presented. Table 5 represents the input values of the CCHP cycle.

Results of energy and exergy efficiency of this cycle are shown in Table 6.

Table 6. Energy and exergy efficiency results of the cycle

Efficiency	Value (%)
Energy efficiency of CHP in scenario one	86.54%
Energy efficiency of CCHP in scenario one	87.85%
Energy efficiency of CHP in scenario two	90.59%
Energy efficiency of CCHP in scenario two	91.9%
Exergy efficiency of CHP in scenario one	86.66%
Exergy efficiency of CCHP in scenario one	86.61%
Exergy efficiency of CHP in scenario two	86.03%
Exergy efficiency of CCHP in scenario two	85.98%

The carbon dioxide consumption factor refers to a portion of carbon dioxide traveling from cathode to anode. Fig. 4 shows changes in electrical efficiency and voltage drop versus the carbon dioxide consumption factor. As can be seen, increasing the carbon dioxide utilization factor has a detrimental effect on the voltage and efficiency of the MCFC, which is apparent and meaningfully notice-

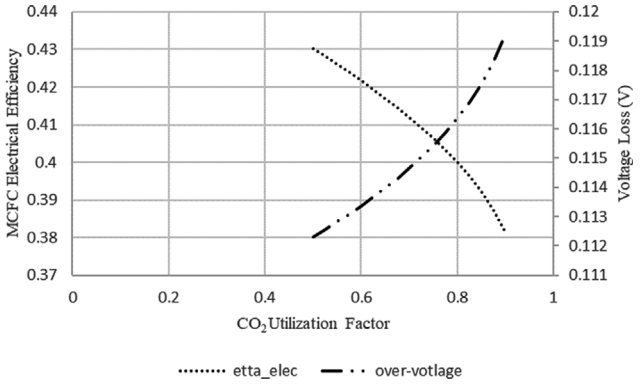

Fig. 4. Changes in voltage drop and efficiency of the molten carbonate fuel cell versus changes in carbon dioxide consumption factor.

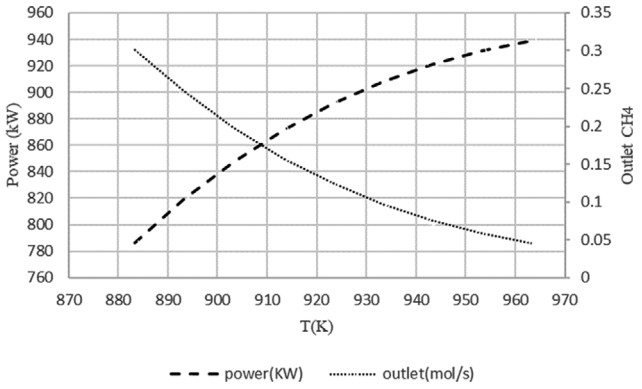

Fig. 5. Changes of unburned methane and output power of the molten carbonate fuel cell versus temperature increment.

able. This trend is comparable to reference [27].

Fig. 5 illustrates the variation in the output power and methane flow rate of molten carbonate fuel cells. Reducing overvoltage in the fuel cell results in an increase in the output power of the fuel cell as the temperature rises. On the other hand, as the temperature rises, much methane is converted to hydrogen, resulting in a decrease in the amount of unconverted methane—consequently, the output methane flow rate decreases.

Furthermore, an increase in the temperature of the MCFC leads to a significant increment in the temperature of fuel cell exhaust gases. Resultantly, output heat from the fuel cell increases, which in turn causes an increase in the energy efficiency of both CHP and CCHP systems in scenario one. This trend is observable in Fig. 5.

Considering that scenario two considers the output energy of the PEM fuel cell, an upward trend in the energy efficiency of this scenario has been evaluated in Fig. 6.

As can be seen, when the temperature of the MCFC increases, the energy efficiencies of both scenario one and scenario two increase, assuming the power and heat of the PEM fuel cell are constant.

In Fig. 7, changes in hydrogen consumption factor versus changes in M-factor have been evaluated. As demonstrated in the figure, an increase in the hydrogen consumption factor is associated with a significant decrease in the amount of the M-factor. This figure is

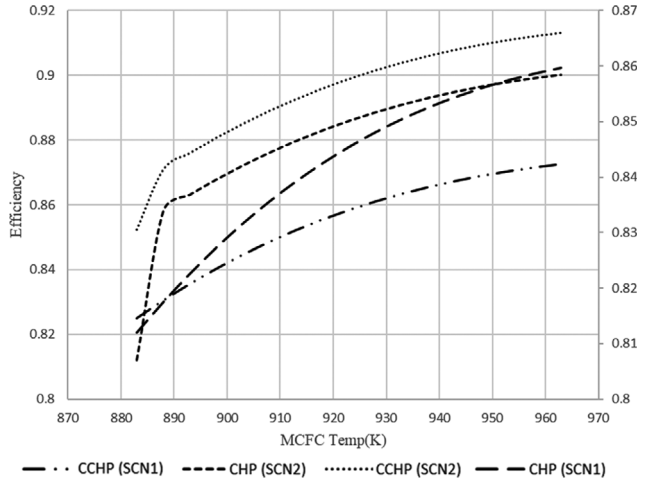

Fig. 6. Changes in system efficiency versus temperature changes in molten carbonate fuel cell in four scenarios (SCN1 to 4).

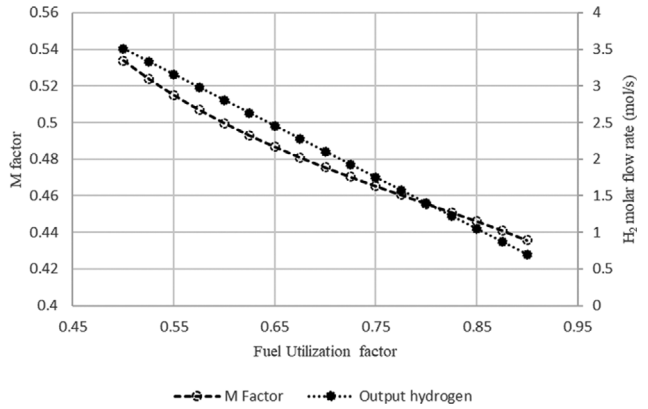

Fig. 7. Changes in M-factor and hydrogen discharge of molten carbonate fuel cell output versus changes in fuel utilization factor.

evaluated through four scenarios (SCN). According to the downward trend of the M-factor, the denominator of the fraction is significantly greater than the numerator, implying that an increase in the fuel consumption factor results in a significant increase in power and heat. As the fuel consumption factor increases, more electrons are released, causing an increase in the current and hydrogen oxidation. According to the figure, this oxidation leads to a decrease in the output hydrogen, and as a result, the output power and heat increase; hence, the trend of the M-factor declines.

Fig. 8 shows a growing trend of both energy and exergy efficiencies with changing in the hydrogen consumption factor. As can be seen, with an increase in the hydrogen consumption factor, both energy and exergy efficiencies show an upward trend resulting from an increase in power and temperature. In the same way, a rising trend toward irreversibility in CHP and CCHP causes an increase in exergy destruction. Moreover, the exergy efficiency of CCHP is lower than that of CHP. According to the obtained results, the highest exergy destruction rates were related to the molten carbonate fuel cell, the polymer fuel cell, and the absorption chiller, respectively.

Results of the economic analysis are in Table 7.

As demonstrated in Table 7, the second scenario receives more

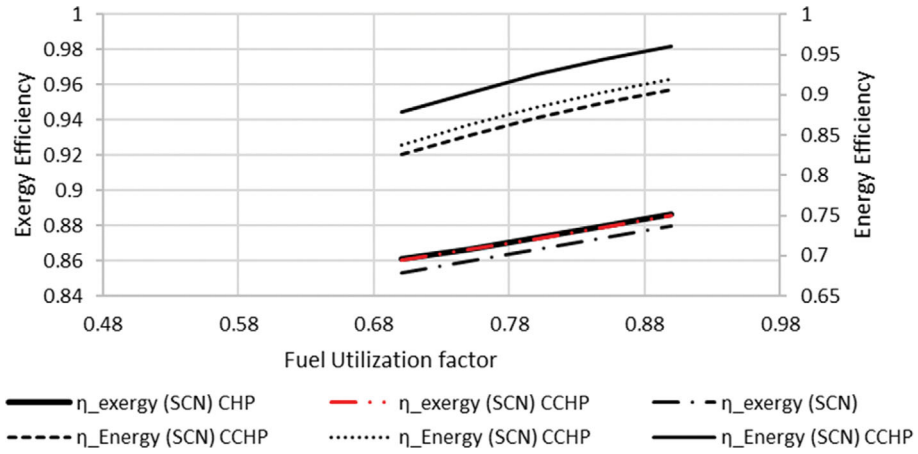

Fig. 8. Changes in energy and exergy efficiencies of the cycle versus fuel utilization factor.

Table 7. Results of economic analysis

SCN	EE	NPV	Tenth-year repayment with/without a scrap	Monthly repayment	25 years of scrap value	PV	FV	DPP	PB	Annual profit
1	6.2	9.4395×10^6	4.6993×10^6 /4.7991×10^6	3.59964×10^4	9.97695×10^4	1.8087×10^6	4.799081×10^6	3.3	4.1	9.88134×10^5
2	6.3	9.8803×10^6	4.8657×10^6 /4.969×10^6	3.81315×10^4	1.03301×10^5	1.8728×10^6	4.968976×10^6	3.2	3.9	1.03496×10^6
3	6.3	9.9847×10^6	4.8657×10^6 /4.969×10^6	3.81315×10^4	1.03301×10^5	1.8728×10^6	4.968976×10^6	3.1	3.1	1.0348×10^6

Table 8. Output results of risk and reliability analyses of the CCHP system components

	MCFC			PEMFC			Absorption Chiller		
	MTTF	The minimum expectation of failure	Reliability in the first failure	MTTF	The minimum expectation of failure	Reliability in the first failure	MTTF	The minimum expectation of failure	Reliability in the first failure
Poor-operation Performance	6082.4	6	36.5%	4033.7	7	36.7%	33251.3	5	69%
Average-operation Performance									
Good-operation	19459.7	10	36.7%	14074.1	7	36.8%	86104	8	36.5%
Performance	33788.1	9	36.7%	23287.1	6	36.7%	146517.4	9	36.7%

attention in comparison with scenarios one and three due to the obtained higher annual profit. Furthermore, considering that only the MCFC is used in scenario one, the annual profit and economic efficacy are lower than the second and third ones. In the second scenario, a polymer fuel cell is used to reuse the output hydrogen of the molten carbonate, and the rest of the hydrogen is collected in a storage tank.

In the third scenario, given that the hydrogen required for the polymer fuel cell must be purchased from the network, it will lead to a lower annual profit compared to the second scenario and, due to the increased power and heat, a higher annual profit compared with the first scenario.

The investor of this cycle, if necessary, can apply for a loan with a simple or compound repayment. As shown in Table 7, by running the second scenario, the monthly repayment will increase by less than $4,000 compared to the first scenario. NPV can also be considered as an evaluation criterion to sort out scenarios, but given that the annual profit obtained from the second scenario is higher than that from the third one, hence, the second scenario has priority.

Importantly, long-term used devices can be sold as scraps after

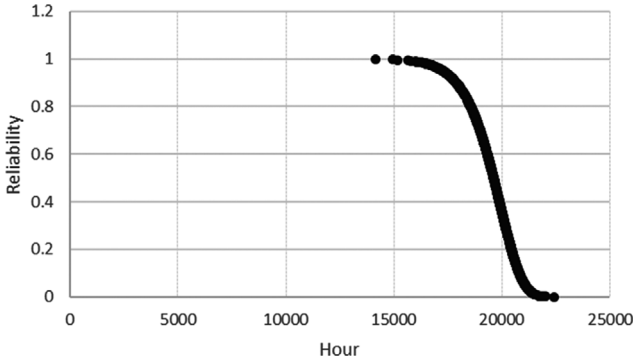

Fig. 9. Changes in the reliability of molten carbonate fuel cells as operating hours are increased.

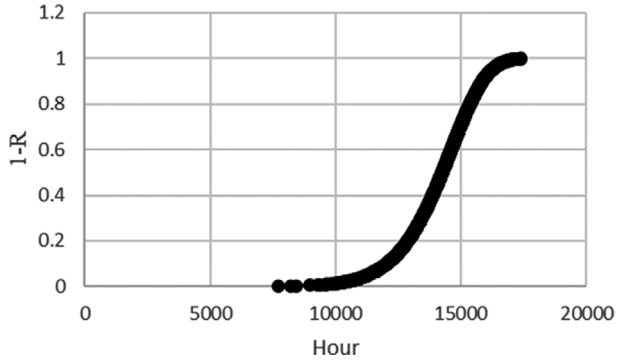

Fig. 10. Weibull cumulative distribution function change versus polymer fuel cell operating hours.

the end of their service life. A coefficient of scrap has been assumed at 0.01, and a compound payback period has been presented following and without the scrap value.

Table 8 shows the complete results of risk and reliability analyses.

The mean time to the first failure, the minimum number of failures, and the operational reliability of the devices have been assessed separately in Table 8.

According to the table, the highest number of expected failures will be related to the molten carbonate fuel cell, the absorption chiller, and the polymer fuel cell, respectively.

The reliability of each component indicates the probability of its operation which could run properly. This probability decreases by increasing the operating hours of the device, which causes a reduction in the life of a device. Because of the similarity of graph trends, only one parameter in average-operation performance has been presented for each component. Figs. 9 to 11 show the reliability of the molten carbonate fuel cell, the cumulative function of the polymer fuel cell, and the number of absorption chiller failures versus the operating hours in the average-operation performance, respectively.

Fig. 9 illustrates a trend of reliability changes with an increase in operating hours related to the average-operation of the molten carbonate fuel cell. As can be seen, an increase in operating hours of the MCFC leads to an increase in the age of the system and, thus, the reliability of the molten carbonate fuel cell decreases and approaches zero by 22431 operating hours.

As shown in Fig. 9, before reaching 14,160 operating hours, the molten carbonate fuel cell is working properly with 100% of reliability, while by approaching 14,160 operating hours, the reliability of the fuel cell declines from 100% to 99%, and then gradually decreases with a downward trend. On the other hand, the probability that the molten carbonate fuel cell is working properly at 19,622 operating hours is expected to be 50%. This figure depicts the same trend of change for all three components and three modes of operations: poor, average, and good.

Fig. 10 shows a cumulative distribution function of the polymer fuel cell versus average-operation performance. A cumulative distribution function fully describes how the random and discrete variables are distributed. In contrast to the reliability distribution, this function has an upward trend due to approaching 100% reliability. The trend of changes in this figure is the same for all three components and the three modes of operation: poor, average, and good.

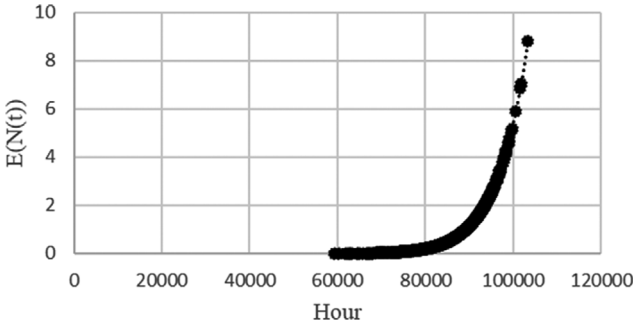

Fig. 11. Changes in the expected number of failures versus operating hours of a single-effect absorption chiller.

Fig. 11 depicts the expected minimum failures of the absorption chiller versus the number of operating hours in average-operation performance. As can be seen, by increasing the operating hours of the absorption chiller, the number of failures of the device increases significantly. With a closer examination of the figure, it is apparent that no failures have been reported up to 59,325 working hours and that the device operates correctly with a probability of 99.7% and without defects. According to the graph, the first failure of the device occurs during 89,217 working hours, and considering the drawn distribution, the absorption chiller is expected to experience at least nine failures by the end of its life. The trend of changes in this figure is the same for all three components and the three modes of operation: poor, average, and good.

CONCLUSION

This study examined a CCHP system with a molten carbonate fuel cell as the prime mover. The system consisted of a molten carbonate fuel cell, an absorption chiller, a polymer fuel cell introduced in scenarios two and three, and hydrogen and heat storage tanks. Energy and exergy analyses were also performed to evaluate the energy and exergy efficiencies of the cycle. M-factor was introduced and analyzed to assess the power and heat of the molten carbonate fuel cell. System reliability and risk assessments were performed for each component to determine the number and hours of failures.

Additionally, this analysis established when and how much trust can be placed in the system's ability to avoid any failure. Assessing

the economic analysis was based on effective parameters, such as payback period under normal and inflationary conditions, NPV, TRV, annual profit, and economic efficiency. The major findings of this research are:

- The molten carbonate fuel cell produced 891.57 kW of power, which was evaluated concerning the load. The CCHP system's energy and exergy efficiencies were calculated to be 87.85 and 86.62%, respectively, in scenario one, and the molten carbonate fuel cell had the highest rate of exergy destruction.
- With increasing the carbon dioxide consumption factor, the overvoltage increased and, consequently, the electrical efficiency of the molten carbonate fuel cell decreased significantly.
- As the molten carbonate fuel cell temperature increased, the unused methane flow rate decreased, but the output power from the molten carbonate fuel cell followed an upward trend.
- The M-factor was introduced as a new parameter to assess power and heat changes simultaneously. By increasing the fuel consumption factor, the M-factor and the output hydrogen of the MCFC decreased.
- Payback period was evaluated in various scenarios for recovering hydrogen from molten carbonate. The results indicated that when the inflation rate was considered, the calculated DPP for scenarios one, two, and three was 3.3, 3.2, and 3.1 years, respectively. In the second scenario, the annual profit outperformed scenarios one and three.
- Given that efficiency is defined as a ratio of output to input, the economic efficiency of the cycle was defined as a ratio of annual profit to annual expenses. This efficiency was the same for scenarios two and three.
- Because most banks calculate loans using a compound payback period schedule, this type of repayment was evaluated both following and without considering the scrap value of each component at the end of its life. The payback period in scenario one was less than that in scenarios two and three; however, the scrap value of components was higher in scenarios two and three.
- As the operating hours of the system increased in each of the three modes of operation (poor, average, and good), the reliability of each component decreased and the number of component failures increased.
- The molten carbonate fuel cell, the polymer fuel cell, and the absorption chiller will all fail at least 10, 7, and 8 times, respectively, if their average operating hours follow a Weibull distribution trend.
- MTTF for the aforementioned components with a distribution of average-operation working hours will be 19,459.7, 140,741, and 86,104 hours, respectively.

Finally, future research should analyze and evaluate this CCHP system using molten carbonate and solid oxide fuel cells (SOFC). With consideration of cooling and heating loads of a building, the research becomes more appealing.

REFERENCES

1. M. Sheykhi, M. Chahartaghi, M. M. Balakheli, B. A. Kharkeshi and S. M. Miri, *Energy Convers. Manag.*, **180**, 183 (2019).
2. M. Sheykhi, M. Chahartaghi, M. M. Balakheli, S. M. Hashemian, S. M. Miri and N. Rafiee, *Energy Convers. Manag.*, **185**, 291 (2019).
3. Z. Liu and I. A. Karimi, *Energy Convers. Manag.*, **171**, 1675 (2018).
4. M. Wu, H. Zhang and T. Liao, *Int. J. Hydrogen Energy*, **42**(51), 30156 (2017).
5. J. H. Ahn, J. H. Jeong and T. S. Kim, *J. Eng. Gas Turbines Power*, **141**(4), 041036 (2019).
6. M. Marefati, M. Mehrpooya and M. B. Shafii, *Energy Convers. Manag.*, **183**, 193 (2019).
7. D. Roy, S. Samanta and S. Ghosh, *J. Brazilian Soc. Mech. Sci. Eng.*, **41**(3), 112 (2019).
8. B. Ghorbani, M. Mehrpooya and S. A. Mousavi, *J. Clean. Prod.*, **220**, 1039 (2019).
9. J. Wang, Y. Chen, N. Lior and W. Li, *Energy*, **185**, 463 (2019).
10. M. Rajabi, M. Mehrpooya, Z. Haibo and Z. Huang, *Appl. Energy*, **253**, 113544 (2019).
11. L. Mastropasqua, L. Pierangelo, M. Spinelli, M. C. Romano, S. Campanari and S. Consonni, *Int. J. Greenh. Gas Control*, **88**, 195 (2019).
12. S. Erzen, E. Açıkkalp and A. Hepbasli, *Int. J. Hydrogen Energy*, **44**(42), 23741 (2019).
13. A. Salehi, S. M. Mousavi, A. Fasihfar and M. Ravanbakhsh, *Int. J. Hydrogen Energy*, **44**(59), 31488 (2019).
14. M. Spinelli, D. Di Bona, M. Gatti, E. Martelli, F. Viganò and S. Consonni, *J. Power Sources*, **448**, 227223 (2020).
15. E. Açıkkalp, L. Chen and M. H. Ahmadi, *Energy Rep.*, **6**, 10 (2020).
16. T. Wejrzanowski, K. Cwieka, J. Skibinski, A. Lysik, S. Haj Ibrahim, J. Milewski, W. Xing and C.-G. Lee, *Int. J. Hydrogen Energy*, **45**, 25719 (2019).
17. J.-Y. Ryu, Ar. Ko, S.-H. Park and J.-P. Park, *Appl. Therm. Eng.*, **169**, 114911 (2020).
18. J. Ahn, S. H. Park, S. Lee, Y. Noh and D. Chang, *Int. J. Hydrogen Energy*, **43**(15), 7525 (2018).
19. X. Guo, H. Zhang, J. Zhao, F. Wang, J. Wang, H. Miao and J. Yuan, *Int. J. Ambient Energy*, **43**, 1986 (2020).
20. R. Chacartegui, B. Monje, D. Sánchez, J. A. Becerra and S. Campanari, *Int. J. Greenh. Gas Control*, **19**, 453 (2013).
21. J. Wang, Y. Liu, F. Ren and S. Lu, *Energy*, **197**, 117313 (2020).
22. J. Rosen, T. Geary, A. Hilmi, R. Blanco-Gutierrez, C.-Y. Yuh, C. S. Pereira, L. Han, R. A. Johnson, C. A. Willman and H. Ghezel-Ayagh, *J. Electrochem. Soc.*, **167**(6), 064505 (2020).
23. M. Y.-P. Peng, C. Chen, X. Peng and M. Marefati, *Sust. Energy Technol. Assessments*, **39**, 100713 (2020).
24. M. Chahartaghi and B. A. Kharkeshi, *Appl. Therm. Eng.*, **128**, 805 (2018).
25. M. Chahartaghi, M. Einanlou and S. M. Hashemian, *Appl. Therm. Eng.*, **193**, 116989 (2021).
26. J. P. Pérez-Trujillo, F. Elizalde-Blancas, S. J. McPhail, M. Della Pietra and B. Bosio, *Appl. Energy*, **263**, 114630 (2020).
27. S. Campanari, P. Chiesa and G. Manzolini, *Int. J. Greenh. Gas Control*, **4**(3), 441 (2010).
28. H. Hongliang, H. Zhang, S. Weng and M. Su, *J. Power Sources*, **161**(2), 849 (2006).
29. M. Baranak and H. Atakül, *J. Power Sources*, **172**(2), 831 (2007).
30. P. Zhao, J. Wang, L. Gao and Y. Dai, *Int. J. Hydrogen Energy*, **37**(4), 3382 (2012).
31. M. Chahartaghi and M. Sheykhi, *Energy*, **174**, 1251 (2019).

32. X. Zhang, R. Zeng, Q. Deng, X. Gu, H. Liu, Y. He, K. Mu, X. Liu, H. Tian and H. Li, *Energy Convers. Manag.*, **199**, 111953 (2019).
33. R. E. Sonntag, C. Borgnakke, G. J. Van Wylen and S. Van Wyk, *Fundamentals of thermodynamics*, 6th ed., vol. 6. Wiley New York (1998).
34. http://www.exergoecology.com/excalc.
35. C. Beggs, *Energy: management, supply, and conservation*, Routledge (2010).
36. H. J. Stone, D. Paul, S. Millett, G. Hund, K. Mahadevan and K. Judd, Economic Analysis of Stationary PEMFC Systems, 961 (2007).
37. K. Mahadevan, V. Contini, M. Goshe, F. Eubanks and F. Griesemer, *2010 Annu. Merit Rev. Proceedings, Dep. Energy Hydrog. Fuel Cells Progr.*, 693 (2010).
38. D. Roy, S. Samanta and S. Ghosh, *Energy Convers. Manag.*, **211**, 112740 (2020).
39. M. Abbasi, M. Chahartaghi and S. M. Hashemian, *Energy Convers. Manag.*, **173**, 359 (2018).
40. D. Kumar, *Tutorials on Life Cycle Costing and Reliability Engineering* (2008).